Carbohydrate Polymers 98 (2013) 905–913

Contents lists available at SciVerse ScienceDirect

Carbohydrate Polymers

journal homepage: www.elsevier.com/locate/carbpol

One-step synthesis of amphiphilic hyperbranched amylopectin derivatives, characterization and use as functional nanovehicles

Di Zeng, Jizhou Fan, Zhibin Deng, Jiayun Tan, Zheng Deng, Li-Ming Zhang, Liqun Yang*

Institute of Polymer Science, Key Laboratory of Designed Synthesis and Application of Polymer Material, Key Laboratory for Polymeric Composite and Functional Materials of Ministry of Education, School of Chemistry and Chemical Engineering, Sun Yat-Sen University, Guangzhou 510275, China

ARTICLE INFO

Article history:
Received 19 April 2013
Received in revised form 11 June 2013
Accepted 3 July 2013
Available online 9 July 2013

Keywords:
Amylopectin
Hyperbranched polysaccharide
Nanovehicle
Controlled release
Metallic nanoparticle

ABSTRACT

Amylopectin is a naturally hyperbranched biopolymer with an extremely high molecular weight. Furthermore, this material is non-toxic in nature, and exhibits good biocompatibility and biodegradability properties. Herein, we describe the development of a one-step reaction strategy for the synthesis of amphiphilic high-molecular-weight hyperbranched amylopectin derivatives with hydrophobic shells and large hydrophilic cores. The chemical structures of the resulting materials were characterized using FTIR spectroscopy, solid-state ^{13}C cross-polarization/magic angle spinning NMR spectroscopy and gas chromatography. The results from transmission electron microscopy, fluorescence spectroscopy, and UV–vis analysis confirmed that the hyperbranched amylopectin derivatives were composed of hydrophobic shells with cholesteryl residues and hydrophilic amylopectin cores. These amylopectin derivatives exhibited high encapsulation capabilities toward water-soluble molecules, and could be used as functional nanovehicles for the controlled release of water-soluble molecules, and the *in situ* synthesis of metallic nanoparticles.

1. Introduction

Hyperbranched polymers have been the subject of considerable levels of attention, because of their unique globular and highly branched structures, which possess a tree-like topology as well as a large number of functional groups (Huang, Su, & Bo, 2009; Seiler, Rolker, & Arlt, 2003; Voit & Lederer, 2009). Amylopectin, which is found in starch granules with amylose, is a natural hyperbranched polysaccharide with an extremely high weight average molecular weight (M_w) of approximately 10^6–10^8 g mol^{-1} (Bello-Perez, Roger, Colonna, & Paredes-Lopez, 1998; Ma, Zhao, Cheng, Zhang, Xu, & Zhang, 2007; Rolland-Sabate, Colonna, Mendez-Montealvo, & Planchot, 2007). The hyperbranched structure of amylopectin is depicted in Fig. 1A-a. Approximately every 20–25 α-D-(1→4) glucose units of its linear chain are interlinked via α-D-(1→6) glycosidic linkage, forming the branch-on-branch topological structure (Miranda, Cacita, & Okano, 2007). At low concentrations (≤ 2 mg/mL) in dimethyl sulfoxide (DMSO) and water, amylopectin exists in a compact spherical conformation with a radius of gyration (R_g) and dynamic radius (R_h) ≈ 100–300 nm (Bello-Perez et al., 1998; Ma et al., 2007; Rolland-Sabate et al., 2007; Yang, Meng, Chen, Liu, Hua, & Ni, 2006).

Recently, it was found that amphiphilic hyperbranched polymers with hydrophobic shells and hydrophilic cores (AHPSCs) could be dissolved in nonpolar solvents to form nanovehicles that readily extracted water-soluble molecules from the aqueous phase into the nonpolar phase (Chen, Shen, Pastor-Prez, Frey, & Stiriba, 2005; Lin, Liu, Dong, Li, Chen, & Li, 2008). Such nanovehicles thus hold great potential for applications such as drug delivery (Jones, Gao, & Leroux, 2008; Jones, Tewari, Blei, Hales, Pochan, & Leroux, 2006) and nanoreactors (Shen, Chen, Frey, & Stiriba, 2006; Slagt, Stiriba, Gebbink, Kautz, Frey, & Koten, 2002; Vriezema, Aragones, Elemans, Cornelissen, Rowan, & Nolte, 2005). AHPSCs are typically synthesized via the partial modification of the surface functional groups of hydrophilic hyperbranched polymers with hydrophobic residues (Chen et al., 2005; Lin et al., 2008; Satoh, 2009). It has been demonstrated that an increase in the size of the AHPSC core leads to an increase in the number of water-soluble molecules that can be encapsulated in the core (Lin et al., 2008; Wiltshire & Qiao, 2007). However, few attempts have been made to synthesize AHPSCs of this particular type, and this has been attributed to the difficulty associated with the synthesis of high-molecular-weight hydrophilic hyperbranched polymers, which results from the high viscosities that exist during the synthetic reaction in the absence of any solvent (Kainthan, Muliawan, Hatzikiriakos, & Brooks, 2006). To date, the molecular weights achievable for synthetic hydrophilic hyperbranched polymers are typically in the range of 10^3–10^5 g mol^{-1} (Hoai, Sasaki, Sasaki, Kaga, Kakuchi, & Satoh, 2011; Kainthan et al., 2006; Wilms,

* Corresponding author. Tel.: +86 20 84110934; fax: +86 20 84112245.
E-mail address: yanglq@mail.sysu.edu.cn (L. Yang).

0144-8617/$ – see front matter © 2013 Elsevier Ltd. All rights reserved.
http://dx.doi.org/10.1016/j.carbpol.2013.07.007

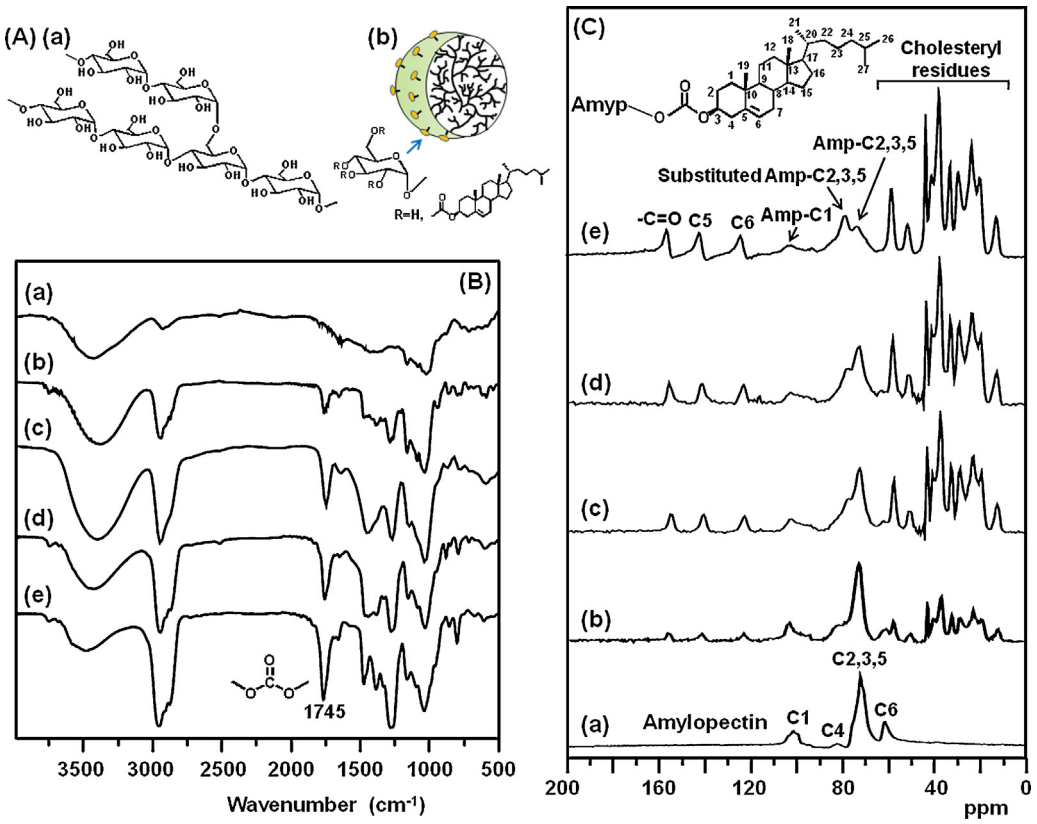

Fig. 1. (A) (a) Chemical structure of amylopectin and (b) schematic structure of amphiphilic hyperbranched amylopectin derivatives. (B) FTIR spectra and (C) solid-state ^{13}C CP/MAS spectra of (a) amylopectin, (b) Amyp-Chol-0.15, (c) Amyp-Chol-0.20, (d) Amyp-Chol-0.23 and (e) Amyp-Chol-0.26.

Wurm, Nieberle, Bohm, Kemmer-Jonas, & Frey, 2009; Wu et al., 2005).

Herein, we describe the development of a one-step reaction strategy for the synthesis of amphiphilic high-molecular-weight hyperbranched amylopectin derivatives with large cores, as illustrated in Fig. 1A-b. According to this strategy, the surface hydroxyl groups of amylopectin were partially modified with bulkily hydrophobic cholesteryl residues. The amylopectin derivatives had a high encapsulation capacity, and were exploited to create nanovehicles for the controlled release of water-soluble molecules and the *in situ* synthesis of metallic nanoparticles.

2. Experimental

2.1. Materials

Amylopectin (from maize), cholesteryl chloroformate (97%) and coumarin 151 (C151, 99%) were purchased from Sigma–Aldrich (St. Louis, MO, USA). Pancreatin from porcine pancreas (P1500), which contains many enzymes, including lipase, amylase, trypsin, ribonuclease and protease, was obtained from Sigma–Aldrich (Poole, UK). DMSO was dried by soaking in molecular sieves and calcium hydride for a week before use. All other chemical reagents were used without further purification.

2.2. Determination of molecular parameters of amylopectin by static light scattering analysis

Light scattering measurements were performed with a static laser scattering system (BI-200SM, Brookhaven Instruments Corporation, NY, USA) at 25 °C and a wavelength of 532.0 nm. The sample solutions were prepared by dissolving amylopectin in DMSO (0.5–5.0 mg/mL), with the resulting solutions being filtered through a membrane filter (nominal pore sized 0.45 μm). The scattering angles were varied from 30° to 150°. The refractive index increment (dn/dc) value was determined to be 0.0648 cm^3/g. The M_w and R_g values were determined using the Berry method based on the Rayleigh–Gans–Debye theory for light scattering according to Eq. (1) as follows:

$$\left(\frac{Kc}{R_\theta}\right)^{1/2} = \left(\frac{1}{M_w}\right)^{1/2}\left[1+\frac{16\pi^2 n^2}{3\lambda^2}R_g^2\sin^2\left(\frac{\theta}{2}\right)\right]^{1/2}(1+A_2M_wc) \quad (1)$$

where the optical constant $K=[4\pi^2n^2(dn/dc)^2]/(N_A\lambda^4)$, n is the refraction index of the solvent, θ is the observation angle, λ is the wavelength of the laser under vacuum conditions, N_A is Avogadro's number, and c is the concentration of the polymer solution. The Rayleigh ratio can be defined by Eq. (2) as follows:

$$R_\theta = \frac{I_\theta r^2}{I_0} \quad (2)$$

where I_0 and I_θ are the intensities of the incident light and the scattered light, respectively, and r is the distance from the light source to the measuring point. A plot of $(Kc/R_\theta)^{1/2}$ against $[\sin^2(\theta/2)+kc]$ can be used to determine the molecular parameters (where k is an arbitrary constant). The square root of the M_w can be obtained from the intercept of the extrapolation to $c=0$ and $\theta=0$. Furthermore, the R_g value can be obtained from the slope of the plots by extrapolating the data to zero angles.

Table 1
Synthesis and characterization of Amyp-Chol derivatives.

Sample[a]	Cholesteryl chloroformate	Triethylamine	DS[b]	$M_{w'}$[c] (10^7 g mol^{-1})
Amyp-Chol-0.15	0.448 g, 1.0 mmol	0.20 g, 2.0 mmol	0.15	4.3
Amyp-Chol-0.20	0.672 g, 1.5 mmol	0.30 g, 3.0 mmol	0.20	4.7
Amyp-Chol-0.23	0.895 g, 2.0 mmol	0.40 g, 4.0 mmol	0.23	4.9
Amyp-Chol-0.26	1.121 g, 2.5 mmol	0.50 g, 5.0 mmol	0.26	5.2

[a] The number following Amyp-Chol is the DS value.
[b] The degree of substitution of cholesteryl residues determined by gas chromatography analysis.
[c] The weight average molecular weight ($M_{w'}$) of the Amyp-Chol was determined based on the M_w of amylopectin: $M_{w'} = M_w \times [1 + (414/162) \times DS]$, where 414 and 162 are the molecular weight of cholesteryl and glucose groups, respectively.

2.3. Synthesis and characterization of the amphiphilic amylopectin derivatives

Amylopectin (0.20 g, 1.2 mmol glucose units) was dissolved in 100 mL of water-free DMSO at 40 °C. 4-Dimethylamino pyridine (1.0 g, 8.2 mmol) together with different amounts of triethylamine and cholesteryl chloroformate were dissolved in 5 mL of chloroform and then added under stirring, as described in Table 1. The reaction was allowed to proceed under an atmosphere of nitrogen at room temperature for 24 h to yield a suspension before being stopped via the addition of 500 mL of the distilled water. The mixture was centrifuged at 25,000 rpm for 10 min to allow for the removal of the triethylamine and 4-dimethylamino pyridine. The resultant precipitate was soaked in 30 mL of ethyl acetate for 2 h, and was filtered to get rid of the produced cholesteryl acid. The purification was run in triplicate. The products were named as Amyp-Chol derivatives. Their chemical structures were characterized by FTIR and solid-state ^{13}C NMR spectroscopy. FTIR measurements were performed using an FTIR analyzer (Nicolet/Nexus 670, Thermo Nicolet Corporation, WI, USA), at a resolution of 4 cm^{-1}, using the KBr method. Solid-state ^{13}C NMR experiments were carried out on a superconducting Fourier transform nuclear magnetic spectrometer (AVANCE AV 400, Bruker, Inc., Fallanden, Switzerland), using cross-polarization/magic angle spinning (CP/MAS) technology. The degree of substitution (DS) of the cholesteryl residues on the amylopectin, which is defined as the number of cholesteryl residues per glucose unit of glycogen, was determined using gas chromatography (Supplementary data).

2.4. Characterization of amphiphilic hyperbranched structures of amylopectin derivatives

2.4.1. Transmission electron microscopy (TEM)

A sample was prepared by dissolving 5 mg of Amyp-Chol-0.23 in 1 mL of sunflower seed oil (SFSO). This solution was then added to 9 mL of tetrahydrofuran (THF). The resulting sample solution was dropped on to a 200-mesh carbon-coated copper grid, before being dried in the air, and then negative-dyed by a phosphotungstic acid solution (about 2 wt %) for 30 s. The morphology of Amyp-Chol-0.23 was observed on a transmission electron microscope (JEM-1400, High Contrast, JEOL Ltd., Tokyo, Japan).

2.4.2. Fluorescence spectroscopy of C151 probe

Following the dissolution of the amylopectin derivative (20 mg) in 250 mL of ethyl oleate, the C151 solution (0.5 μL, 0.5 mg/mL) was added, and the resulting mixture was stirred for 6 h. The fluorescence was measured with a Shimadzu RF-5301 PC fluorescence spectrophotometer (Kyoto, Japan).

2.4.3. Detection of dye phase transfer using UV–vis spectroscopy

The amylopectin derivative (2.5 mg) was dissolved in 5 mL of SFSO with stirring at room temperature over a period of 12 h, prior to the addition of 5 mL of an aqueous solution of Congo red (0.1 mg/mL). The resulting mixture was then stirred at room temperature for 10 h, and left to stand for 10 min until the two phases were clearly separated. The dyes dissolved in the oil and aqueous phases were photographed and analyzed using a UV–vis spectrophotometer (UV-3150, Shimadzu Corporation, Kyoto, Japan). In the same way, methyl orange phase transfer was detected.

2.5. Determination of the encapsulation capacity of the Amyp-Chol derivatives for Congo red

2.5.1. Influence of encapsulation time on encapsulation capacity

The Amyp-Chol derivative (2.5 mg) was dissolved in 5 mL of SFSO with stirring at room temperature over a period of 12 h, prior to the addition of 5 mL of an aqueous solution of Congo red (0.2 mg/mL) with stirring. At predetermined time intervals, the two phases were separated and a 0.02 mL sample of the aqueous Congo red solution was removed. The amount of Congo red remaining in the water was analyzed at $\lambda = 495$ nm using UV–vis spectroscopy. A working curve linking the Congo red concentration in water and a wavelength of 495 nm was used to evaluate the amount of Congo red in the aqueous phase ($R^2 > 0.999$). The amount of Congo red encapsulated in the Amyp-Chol derivative was calculated from the reduction in the Congo red concentration. The encapsulation capacity, defined as the number of encapsulated Congo red molecules per Amyp-Chol derivative molecule, was then evaluated.

2.5.2. Influence of the concentration of Amyp-Chol derivative on the encapsulation capacity

Different weights of the Amyp-Chol derivatives (in the range of 2.5–52.8 mg) were dissolved in 5 mL of SFSO with stirring at room temperature over a period of 12 h, prior to the addition of 5 mL of an aqueous solution of Congo red (1.2 mg/mL). The resulting mixtures were then stirred at room temperature for 10 h, and then left to stand until the two phases were separated. The encapsulation capacity was determined using UV–vis spectroscopy, as mentioned above.

2.6. Controlled release of Congo red from the Amyp-Chol nanovehicles

The Amyp-Chol derivative (2.5 mg) was dissolved in 5 mL of SFSO under stirring at room temperature for 12 h. An aqueous Congo red solution (5 mL, 0.2 mg/mL) was then added, and the resulting mixture was stirred for 10 h. The oil phase was then removed and mixed under stirring with 150 mL of phosphate buffer saline (PBS) solution (pH 6.8) containing 1% of pancreatin (w/v). At predetermined time intervals, after the two phases were separated, 1.0 mL of the aqueous solution was removed, and replaced with 1.0 mL of the release solution. The amount of released Congo red in the aqueous phase was analyzed using UV–vis spectroscopy, as mentioned above. The cumulative release of Congo red was then estimated by dividing the weight of the released Congo red by the weight of the Congo red encapsulated in the Amyp-Chol

derivatives. The Congo red release behaviors were also studied in the PBS solution (pH 6.8), in the absence of pancreatin.

2.7. In situ synthesis and characterization of silver nanoparticles in the Amyp-Chol nanovehicles

The Amyp-Chol derivatives (20 mg) were dissolved in 5 mL of SFSO by stirring at room temperature for 12 h, and 2 mL of an aqueous $AgNO_3$ solution (0.01 mmol/mL) was then added under stirring. The reaction was allowed to proceed at room temperature for 48 h, and the reaction solution was then left to stand until the two phases were separated. The silver nanoparticles in the oil phase were analyzed using UV–vis spectroscopy and TEM analysis (without any dye) by adding 1 mL of THF to 1 mL of the oil solution. The solid composite of the silver nanoparticles and the Amyp-Chol derivatives was precipitated via the addition of 100 mL of THF, followed by a period of centrifugation (5000 rpm, 20 min), and drying at 40 °C under vacuum overnight. The X-ray diffraction (XRD) measurements were performed at a scanning speed of $2\theta = 3°$/min using a DMAX 2200 VPC X-Ray diffractometer (Rigaku Co., Tokyo, Japan). The X-ray radiation Cu Kα1 ($\lambda = 0.15418$ nm) was selected with a quartz monochromator.

2.8. Antibacterial property of the silver nanoparticle/Amyp-Chol composites

Based on a method previously described in the literature (Ma, Yi, & Zhang, 2009), *Escherichia coli* (*E. coli*) was used to test the antibacterial activity of the silver nanoparticles synthesized in the Amyp-Chol nanovehicles. Beef extract (0.5 g), tryptone (1.0 g), sodium chloride (0.5 g), agar (2.0 g) and 100 mL of deionized water were placed into a beaker and heated at 50 °C with stirring until all of the substances had dissolved. The pH of the solution was adjusted to 7.2 with a 1.0 mol/L solution of NaOH. The resulting solution was sterilized using high pressure steam at 100 Pa for 20 min before being cooled to approximately 50 °C to form a solid culture medium in a Petri dish. The *E. coli* solution (200 μL) was then added and shaken to allow for its effective dispersion in the culture medium. The solid composite of the silver nanoparticles and the Amyp-Chol derivatives (1 mg) was then placed on the surface of the culture medium and incubated at 37 °C for 24 h.

3. Results and discussion

3.1. Synthesis and characterization of the Amyp-Chol derivatives

To avoid aggregation effects, the molecular parameters of the native amylopectin were investigated in DMSO. The M_w and R_g values were determined to be 3.1×10^7 g mol^{-1} and 137 nm, respectively, by static light scattering analysis (Fig. 2). These values were found to be similar to those reported in the literature (Ma et al., 2007; Zhong, Yokoyama, Wang, & Shoemaker, 2006).

Cholesteryl chloroformate was selected as a hydrophobic modifier because of its high activity, strong hydrophobicity and considerable steric bulk. These unique properties enabled the cholesteryl chloroformate to react with the surface hydroxyl groups of amylopectin. The reaction was conducted in DMSO at a low amylopectin concentration (2 mg/mL) to avoid the aggregation of the amylopectin, following the literature (Ma et al., 2007). In comparison with the FTIR spectrum of amylopectin (Fig. 1B-a), a new peak appeared at 1745 cm^{-1} in the FTIR spectra of the Amyp-Chol derivatives (Fig. 1B-b–e), which was assigned to the vibration absorption of the —C=O of the carbonate bond (Wu, 1994). Moreover, this peak significantly increased with increasing added amounts of cholesteryl chloroformate, indicating that an increasing number of cholesteryl residues had been conjugated with the amylopectin.

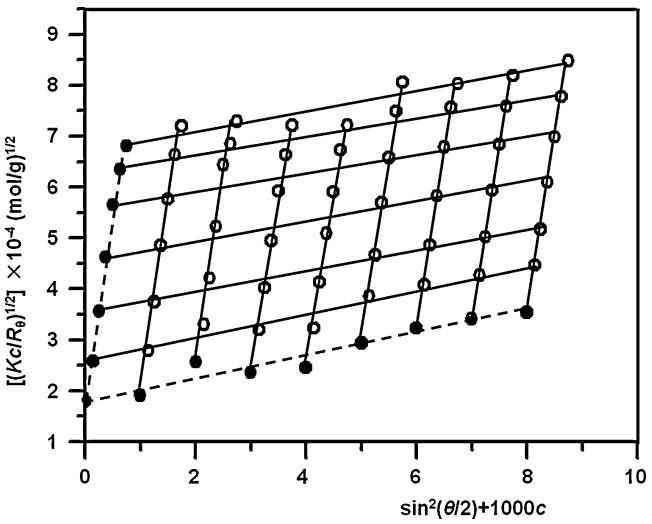

Fig. 2. Berry plots of amylopectin in DMSO (0.5–5.0 mg/mL) at 25 °C.

Considering that the Amyp-Chol derivatives were only soluble in the oil, their chemical structures were characterized using solid-state ^{13}C CP/MAS NMR spectroscopy. In contrast with the solid-state ^{13}C CP/MAS NMR spectrum of amylopectin (Fig. 1C-a), the resonance peaks appeared in the spectra of the Amyp-Chol derivatives are assigned as follows (Fig. 1C-b–e): δ 155.4 (—C=O of carbonate bond), δ 141.5 (C5 of cholesteryl residues), δ 123.4 (C6 of cholesteryl residues), δ 102.3 (C1 of amylopectin), δ 78.2 (cholesteryl residues substituted C2,3,5 of amylopectin), δ 72.8 (C2,3,5 of amylopectin), and δ 60.0–10.0 (cholesteryl residues) (Baik, Dickinson, & Chinachoti, 2003; Guo & Hamilton, 1993; Lesage, Steuerna, & Emsley, 1998). The DS values of the cholesteryl residues were measured quantitatively using gas chromatography (Supplementary data). The Amyp-Chol derivatives were hydrolyzed by a 5 mol/L NaOH solution, and then the produced cholesterol contents were evaluated using gas chromatography with *n*-hexane as a solvent (Fig. S1). The DS values were then determined to be approximately 0.15, 0.20, 0.23 and 0.26 for the four Amyp-Chol derivatives.

3.2. Amphiphilic hyperbranched structures of amylopectin derivatives with hydrophobic shells and hydrophilic cores

Interestingly, the Amyp-Chol-0.23 presented as regular globes following its dissolution in SFSO and THF, as shown in the TEM image (Fig. 3A). This was probably because the hydrophobic cholesteryl residues on the surface of the amylopectin allowed the Amyp-Chol-0.23 to shrink into regular globes in the polar THF, owing to the surface tension. The radii of the Amyp-Chol-0.23 globes were in the range of 100–150 nm. These values were close to the measured R_g value for unimolecular amylopectin, as mentioned above, and these results therefore suggested that the hyperbranched Amyp-Cho-0.23l derivative had a hydrophobic surface and existed in a unimolecular state.

C151 is a well-known fluorescent probe, and is sensitive to the polarity of its local microenvironment (Seth, Chakrabort, Setua, & Sarkar, 2006; Zhang, Yin, Su, & Wu, 2011). That is, its fluorescence emission peaks shift toward the blue as the polarity of the probe microenvironment is decreased. The fluorescence emission spectra of C151 in the different media are shown in Fig. 3B. The emission peak of C151 was at 448 nm in ethyl oleate, and blue shifted to 443 nm in the Amyp-Chol derivatives/ethyl oleate solutions. This result implied that the microenvironment around C151 changed to give more non-polar conditions in the solutions containing the Amyp-Chol derivatives, owing to the hydrophobic interactions

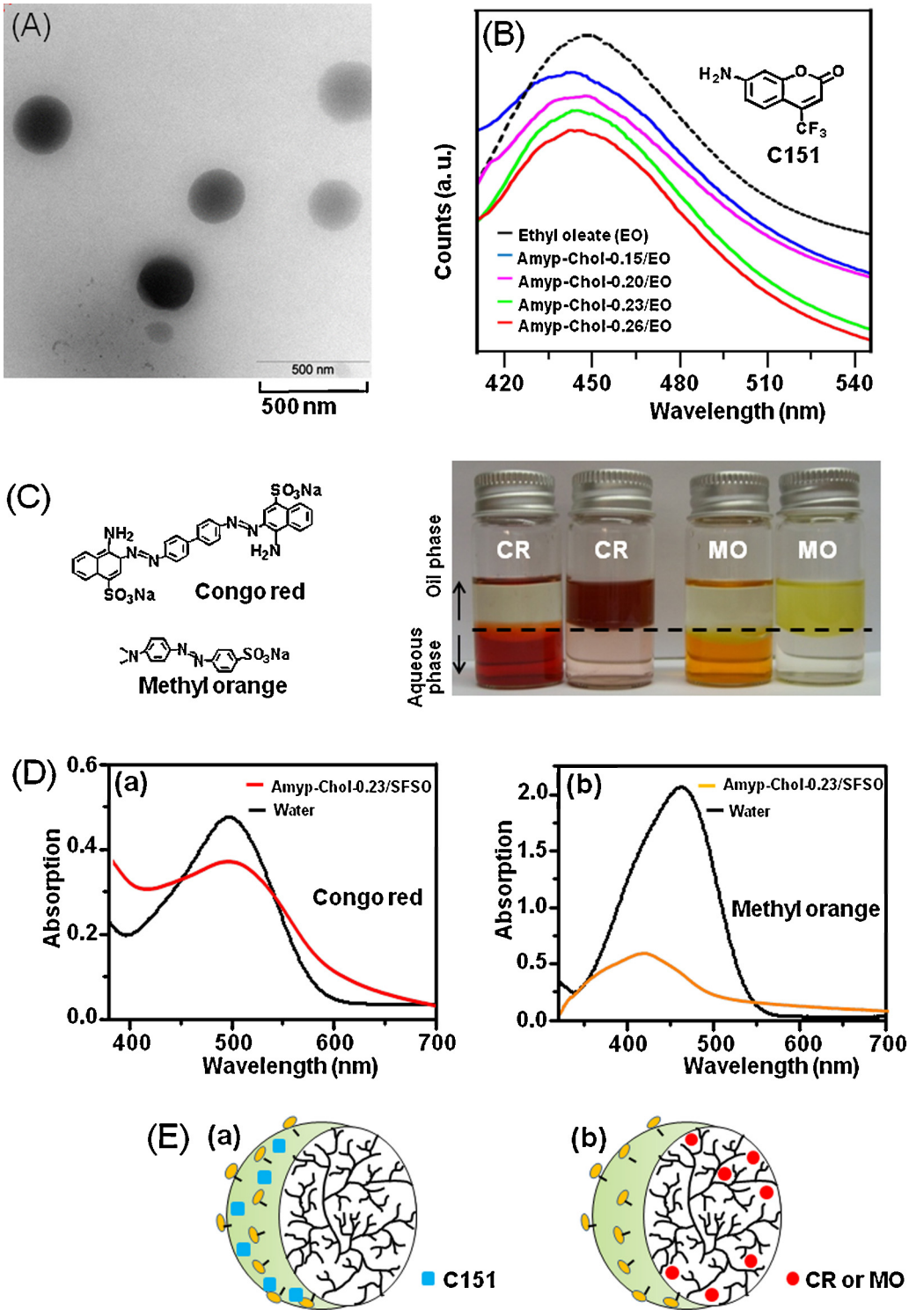

Fig. 3. (A) TEM image of Amyp-Chol-0.23 (0.5 mg/mL) in SFSO/THF (1/9, v/v); (B) fluorescence spectra of C151 in the Amyp-Chol derivatives/ethyl oleate (EO) solutions; (C) phase transfer of water-soluble dyes from the aqueous phase to the oil phase induced by the Amyp-Chol-0.23 derivative (CR: Congo red, MO: methyl orange); (D) UV–vis spectra of water-soluble dyes in the different media: (a) Congo red and (b) methyl orange (with concentration of 0.5 mg/mL for the amylopectin derivatives); (E) schematic interactions of different probes with the amphiphilic hyperbranched amylopectin derivatives.

between C151 and the cholesteryl residues on the surface of the derivatives.

Water-soluble dyes have been widely used to detect the hydrophilic cores and hydrophobic shells of AHPSCs (Chen et al., 2005; Lin et al., 2008; Satoh, 2009). To probe the differences in polarity between the cores and shells in the Amyp-Chol derivatives, the extraction of Congo red and methyl orange from the aqueous phase to the oil phase was carried out. As shown in Fig. 3C, after the Amyp-Chol-0.23 derivative/SFSO solution was stirred with the Congo red aqueous solution at room temperature for 10 h and left to stand for approximately 10 min, the oil phase became red. The phase transition process of Congo red was then monitored using UV–vis spectroscopy (Fig. 3D-a). The maximum absorption wavelength (λ_{max}) of Congo red was at

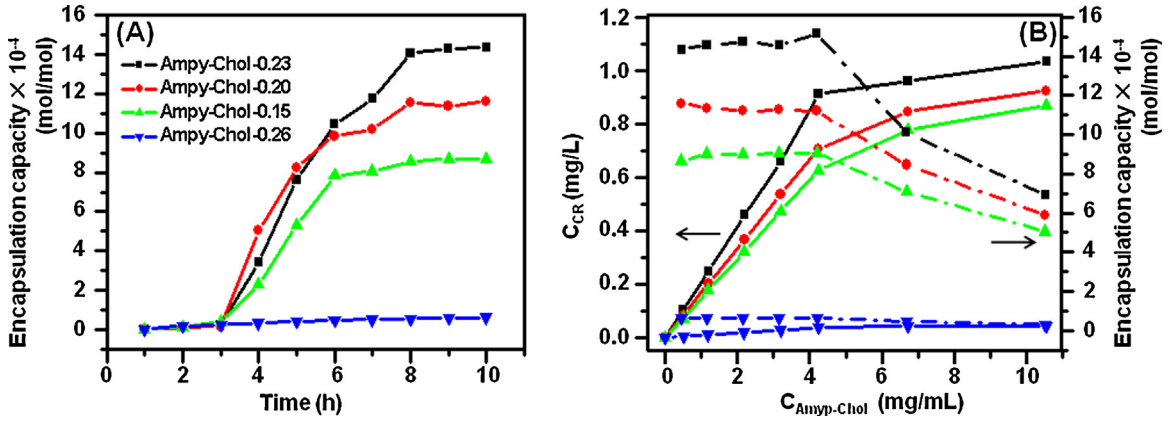

Fig. 4. (A) Dependence of encapsulation capacity of Congo red on time for the Amyp-Chol derivatives in SFSO (0.5 mg/mL); (B) changes of concentration of Congo red with the concentration of the Amyp-Chol derivatives (solid lines), and changes of encapsulation capacity of Congo red with the concentration of the Amyp-Chol derivatives (broken lines) in SFSO (with encapsulation time of 10 h): (■) Amyp-Chol-0.23, (●) Amyp-Chol-0.20, (▲) Amyp-Chol-0.15 and (▼) Amyp-Chol-0.26.

496 nm, in both water and the Amyp-Chol-0.23 derivative/SFSO solution. Supported by the literature (Chen et al., 2005; Lin et al., 2008; Satoh, 2009), these results strongly confirmed that the amylopectin derivatives had hydrophilic cores that supplied a microenvironment suitable for the encapsulation of hydrophilic dye molecules, as well as hydrophobic shells that allowed solvation with the non-polar solvents. The mechanism of the encapsulation of hydrophilic guests by the amylopectin derivatives was attributed to two factors: the first was the interaction between the hydrophilic guests and the groups in the cores of the derivatives, and the second was the compatibility of the hydrophobic derivatives' shells with the non-polar solvent (Zou, Zhao, & Shi, 2006).

Compared with Congo red, methyl orange exhibited greater degree of sensitivity the polarity of the microenvironment (Karukatis, D'Angelo, & Loftus, 1997). We also studied phase transition of methyl orange from the aqueous phase to the oil phase that was induced by the Amyp-Chol-0.23 derivatives. Methyl orange changed from orange to yellow as it moved from the aqueous phase to the oil phase (Fig. 3C). Its λ_{max} value exhibited a blue shift from 460 nm in water to 417 nm in the oil phase (Fig. 3D-b), which coincided with the color change. This demonstrated that the polar microenvironment of water was different from that in the hydrophilic amylopectin cores containing polar hydroxyl groups. These results matched with the literature, which reported the methyl orange absorption wavelength shifted from 462 nm in water to 417 nm in 1-alkanols owing to the stronger polarity of water (Karukatis et al., 1997).

Based on all the aforementioned results, the interactions of different probes with the amphiphilic hyperbranched amylopectin derivatives are illustrated in Fig. 3E-a. The hydrophobic C151 probes may have surrounded the hydrophobic shells of the Amyp-Chol derivatives, but they could not enter the hydrophilic cores, because of their hydrophobicity interactions with the surface cholesteryl residues. In contrast, the water-soluble dyes could pass through the hydrophobic shells and enter the hydrophilic cores (Fig. 3E-b). These results confirmed that the Amyp-Chol derivatives possessed an amphiphilic structure with hydrophobic shells and hydrophilic cores.

3.3. Encapsulation capabilities of amphiphilic hyperbranched amylopectin derivatives for water-soluble molecules

The encapsulation capacity of the amphiphilic hyperbranched polymers for water-soluble molecules is an important property for their applications (Lin et al., 2008; Wiltshire and Qiao, 2007). Using Congo red as a model water-soluble molecule, the encapsulation capacity was determined using UV–vis spectroscopy. Fig. 4A shows the dependence of the Congo red encapsulation capacity on time in SFSO. The encapsulation capacity reached a saturation value when the encapsulation time was longer than approximately 8 h, and the saturation value was in the range of 8.6×10^3 to 1.2×10^4. Furthermore, it was found that the encapsulation capacity increased in the order of Amyp-Chol-0.23 derivative > Amyp-Chol-0.20 derivative > Amyp-Chol-0.15 derivative; i.e., the encapsulation capacity increased with increasing density of cholesteryl residues in the shell. According to the literature (Zou et al., 2006), a possible reason for this is that the Amyp-Chol derivative with a low DS value showed poor compatibility with the SFSO and shrunk into a compact structure, making it difficult for the Congo red molecules to enter into the derivative. However, it is also difficult for the Congo red molecules to enter into the Amyp-Chol-0.26 derivative, because the high shell-density of cholesteryl residues formed an extremely nonpolar surface preventing the Congo red molecules from penetrating the hydrophobic shells. These results indicated that the encapsulation capacity for Congo red was strongly dependent on the shell-density of hydrophobic residues, which agreed with the previous work (Satoh, 2009).

The Congo red encapsulation capacities of different synthetic amphiphilic hyperbranched polymers have been reported in Table 2 (Chen et al., 2005; Lin et al., 2008; Saha & Ramakrishnan, 2009; Stiriba, Kautz, & Frey, 2002). The encapsulation capacities of the amylopectin derivatives for Congo red (8.6×10^3 to 1.2×10^4) were significantly higher than those of the synthetic amphiphilic

Table 2
The Congo red encapsulation capacity and molecular parameters of different synthetic amphiphilic hyperbranched polymers.

Amphiphilic hyperbranched polymer	Molecular weight (g mol^{-1})	R_h (nm)	Encapsulation capacity (mol/mol)
Poly(ester amide)-star-PCL	1.78×10^4 to 8.37×10^4 (M_n[a])	3.19–9.30	0.95–22.6
Amidated polyethylenimine	4.32×10^4 to 1.50×10^5 (M_n)	5–9	16.9–90.1
Polyglycerol palmitoyl ester	8.8×10^3 (M_n)	–	0.9, 1.3
Polyether AB2-TEG-C16	7.0×10^3 (M_n), 1.75×10^4 (M_w)	2.6	2.7

[a] Number average molecular weight.

hyperbranched polymers (0.9–90.1). This difference was attributed to the huge size of the derivatives, which can be explained in terms of the extremely high M_w and large size of the native amylopectin.

The influence of the concentration of the Amyp-Chol derivative on the Congo red encapsulation capacity was further studied in SFSO (Fig. 4B). The concentration of encapsulated Congo red increased proportionally with increasing concentration of Amyp-Chol derivatives, for concentrations lower than approximately 4 mg/mL. As expected, the Congo red encapsulation capacities were almost invariant at these low concentrations. However, the concentration of encapsulated Congo red increased much more slowly, and the Congo red encapsulation capacities decreased, for concentrations higher than approximately 4 mg/mL. Based on related research previously published in the literature (Lin et al., 2008; Satoh, 2009), these results could indicate that the Amyp-Chol derivatives aggregated at high concentrations. The Congo red encapsulation capacity could therefore be related to the existing state of the Amyp-Chol derivatives in the solvent.

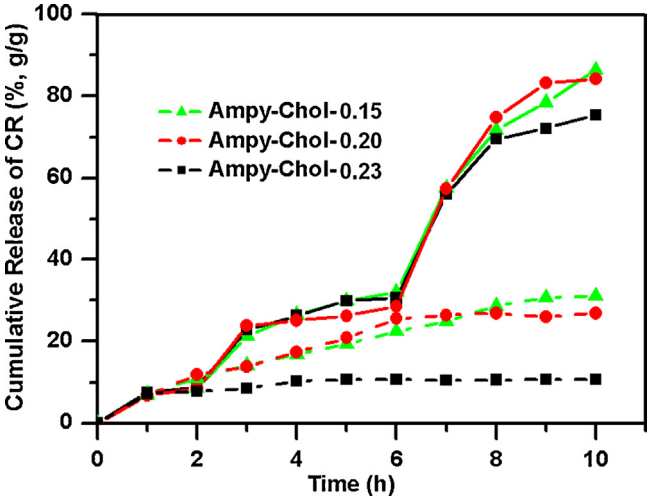

Fig. 5. Release profiles of Congo red from the Amyp-Chol nanovehicles in PBS solution (pH 6.8) (solid lines: in the presence of 1% of pancreatin (w/v); broken lines: without pancreatin).

3.4. Controlled release behaviors of the Amyp-Chol nanovehicles

Amylopectin is a natural polysaccharide with a non-toxic nature, and good biocompatibility and biodegradable properties. In addition, the cholesteryl residues of the Amyp-Chol derivatives confer good biocompatibility, as well as the potential for interactions with the cholesteryl receptors on cell surfaces (Liu, Pramoda, Yang, Chow, & He, 2004). With all of this in mind, the decision was taken to evaluate the potential application of these Amyp-Chol nanovehicles (i.e., the derivatives described above) as drug delivery systems. Congo red was selected as a model drug molecule. The release behaviors were investigated in a PBS solution (pH6.8) containing 1% of pancreatin, which was composed of various enzymes, including lipase and amylase. The release profiles shown in Fig. 5 revealed that approximately 75–90% of the Congo red molecules were released continuously from the Amyp-Chol nanovehicles over a period of 10 h in the presence of pancreatin. The release process included two stages: before 6 h and after 6 h. In the first stage (0–6 h), a small amount of Congo red was released, because the ester bonds between the cholesteryl residue shells and the amylopectin cores were hydrolyzed by the lipase of the pancreatin. In the second stage (6–12 h),

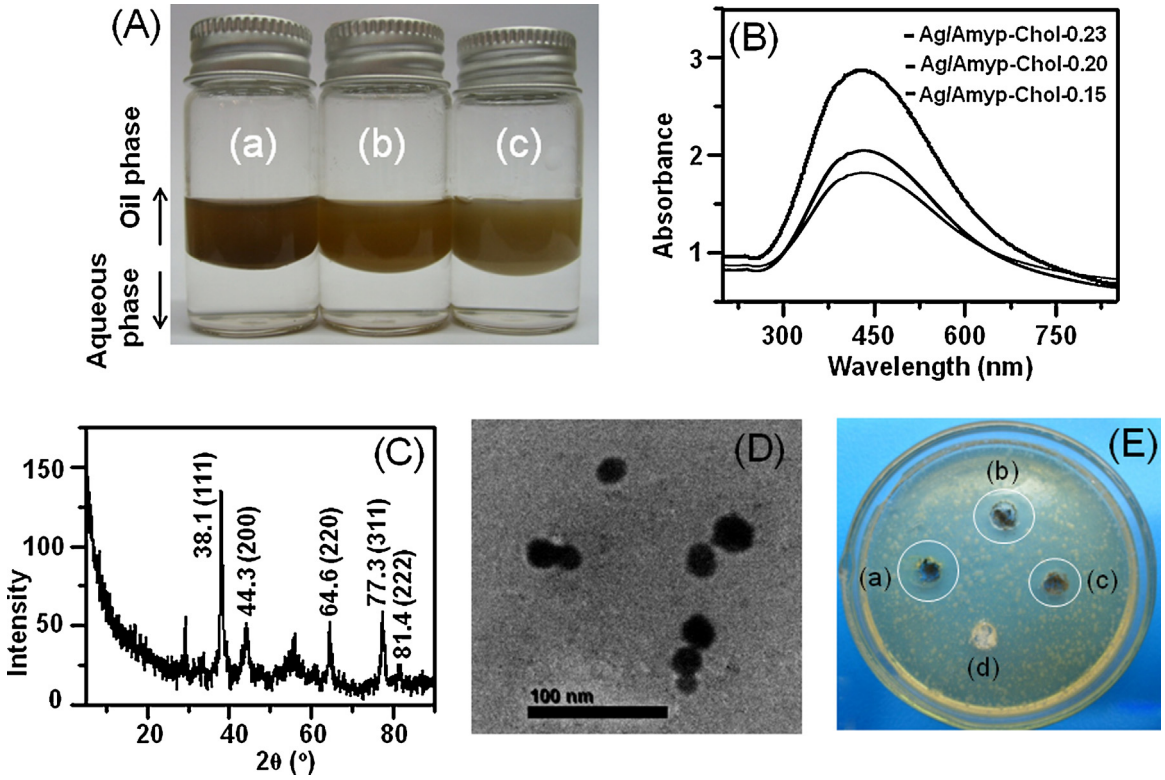

Fig. 6. (A) *In situ* synthesis of silver nanoparticles in the Amyp-Chol nanovehicles: (a) Amyp-Chol-0.23, (b) Amyp-Chol-0.20, (c) Amyp-Chol-0.15; (B) UV–vis spectra of silver nanoparticles in the Amyp-Chol nanovehicles; (C) and (D) XRD pattern and TEM image of the silver nanoparticles in the Amyp-Chol-0.23 nanovehicle; (E) antibacterial property of the Amyp-Chol derivative/silver nanoparticle composites to *E. coli*: (a) Amyp-Chol-0.23/silver nanoparticles, (b) Amyp-Chol-0.20/silver nanoparticles, (c) Amyp-Chol-0.15/silver nanoparticles, and (d) Amyp-Chol-0.23.

the glycosidic linkages of the amylopectin cores were further hydrolyzed by the amylase from the pancreatin. As a result, the Amyp-Chol nanovehicles were collapsed and released Congo red. In contrast, less than 30% of the Congo red molecules were released from the Amyp-Chol nanovehicles in the absence of pancreatin.

3.5. *In situ* synthesis of silver nanoparticles in the Amyp-Chol nanovehicles

To investigate whether the Amyp-Chol derivatives might be used as a chemical-reaction nanovehicle, the *in situ* synthesis of silver nanoparticles was carried out. After the Amyp-Chol derivatives/SFSO solution and an $AgNO_3$ aqueous solution were mixed under stirring for 48 h and left to stand for a while, the oil phase became brown (Fig. 6A). A strong surface plasmon resonance signal centered at 430 nm was observed in the UV–vis spectra of the oil phase as shown in Fig. 6B, implying the formation of silver nanoparticles (Wang, Rubner, & Cohen, 2002). This resulted from the encapsulation of the $AgNO_3$ molecules by the Amyp-Chol nanovehicles in the oil phase, and the subsequent *in situ* reduction of the silver cations by the hemiacetal groups of amylopectin, which yielded silver nanoparticles inside the nanovehicles. Moreover, the absorption of the silver nanoparticles increased as the DS value of the Amyp-Chol derivatives increased, indicating that the silver nanoparticle content had also increased. This result was in agreement with the color change of the silver nanoparticles, as shown in Fig. 6A. In the previous work (Garamus et al., 2004; Wan, Fu, & Huang, 2006), metallic nanoparticles were synthesized in the amphiphilic hyperbranched polymer nanovehicles, using $NaBH_4$ and H_2 as reducing agents. Here, silver cations were reduced *in situ* by the hemiacetal groups of the Amyp-Chol nanovehicles, which is simpler and more feasible for applications.

The XRD pattern of the solid product in the oil phase is shown in Fig. 6C. The peaks observed at $2\theta = 38.1$, 44.3, 64.6, 77.3 and 81.4° were assigned to diffraction from the (1 1 1), (2 0 0), (2 2 0), (3 1 1) and (2 2 2) planes of silver with cubic symmetry (JCPDS, No. 4-0783), further confirming that the product contained metallic silver. Using the Scherer formula provided below (Eq. (3)) (Prakash, Muralidharan, Nallamuth, Venkateswarlu, & Satyanarayana, 2007), the silver nanocrystalline size was calculated to be approximately 10 nm by selecting the parameters of the strongest peak (i.e., $2\theta = 38.1°$). The Scherer formula is as follows:

$$D = \frac{0.9\lambda}{\beta \cos\theta} \quad (3)$$

where λ is the X-ray wavelength (0.15418 nm) and β is the half band width.

Fig. 6D shows a TEM image of the silver nanoparticles synthesized in the Amyp-Chol-0.23 nanovehicle. These particles were spherical in shape with sizes in the range of 10–25 nm, which were very similar to those calculated from the results of the XRD analysis.

Fig. 6E shows the antibacterial effects of the pure Amyp-Chol derivatives and Amyp-Chol derivative/silver nanoparticle composites on *E. coli*. As expected, the colonies surrounding the composites barely grew at all (Fig. 6E-a–c), whereas the Amyp-Chol-0.23 derivative did not show any effect on the growth of *E. coli* (Fig. 6E-d). On the basis of these results, it was concluded that the silver nanoparticles in the composites exhibited excellent antibacterial activity. Moreover, the size of the non-colony area increased as the DS value of the Amyp-Chol derivatives increased, because of the different amounts of silver nanoparticles produced.

4. Conclusions

In conclusion, we have presented a one-step reaction strategy for the synthesis of amphiphilic high-molecular-weight hyperbranched amylopectin derivatives with hydrophobic shells and hydrophilic cores. The large amylopectin cores of the derivatives could encapsulate water-soluble molecules, and showed high encapsulation capacities. These amylopectin derivatives were used as nanovehicles for the controlled release of water-soluble molecules and the efficient *in situ* synthesis of metallic nanoparticles.

Acknowledgments

This work was supported by the National Natural Science Foundation of China (20974130, 21244005 and 20574089) and the Fundamental Research Funds for the Central Universities, China (09lgpy14). The authors thank Professor Lin Ma and Dr. Ling Zhang for assisting with the antibacterial and fluorescence probe experiments.

Appendix A. Supplementary data

Supplementary data associated with this article can be found, in the online version, at http://dx.doi.org/10.1016/j.carbpol.2013.07.007.

References

Baik, M. Y., Dickinson, C., & Chinachoti, P. J. (2003). Solid-State ^{13}C CP/MAS NMR studies on aging of starch in white bread. *Agriculture of Food Chemistry*, *51*, 1242–1248.

Bello-Perez, L. A., Roger, P., Colonna, P., & Paredes-Lopez, O. (1998). Laser light scattering of high amylose and high amylopectin materials, stability in water after microwave dispersion. *Carbohydrate Polymers*, *37*, 383–394.

Chen, Y., Shen, Z., Pastor-Prez, L., Frey, H., & Stiriba, S. E. (2005). Role of topology and amphiphilicity for guest encapsulation in functionalized hyperbranched poly(ethylenimine)s. *Macromolecules*, *38*, 227–229.

Garamus, V. M., Maksimova, T., Richtering, W., Aymonier, C., Thomann, R., Antoniett, L., et al. (2004). Solution structure of metal particles prepared in unimolecular reactors of amphiphilic hyperbranched macromolecules. *Macromolecules*, *37*, 7893–7900.

Guo, W., & Hamilton, J. A. (1993). Molecular organization and motions of cholesteryl esters in crystalline and liquid crystalline phases: A ^{13}C and ^{1}H magic angle spinning NMR study. *Biochemistry*, *32*, 9038–9052.

Hoai, N. T., Sasaki, A., Sasaki, M., Kaga, H., Kakuchi, T., & Satoh, T. (2011). Synthesis, characterization, and lectin recognition of hyperbranched polysaccharide obtained from 1,6-anhydro-D-hexofuranose. *Biomacromolecules*, *12*, 1891–1899.

Huang, W., Su, L., & Bo, Z. (2009). Hyperbranched polymers with a degree of branching of 100% prepared by catalyst transfer Suzuki-Miyaura polycondensation. *Journal of American Chemical Society*, *131*, 10348–10349.

Jones, M. C., Tewari, P., Blei, C., Hales, K., Pochan, D. J., & Leroux, J. C. (2006). Self-assembled nanocages for hydrophilic guest molecules. *Journal of American Chemical Society*, *128*, 14599–14605.

Jones, M. V., Gao, H., & Leroux, J. C. (2008). Reverse polymeric micelles for pharmaceutical applications. *Journal of Controlled Release*, *132*, 208–215.

Kainthan, R. K., Muliawan, E. B., Hatzikiriakos, S. G., & Brooks, D. E. (2006). Synthesis, characterization, and viscoelastic properties of high molecular weight hyperbranched polyglycerols. *Macromolecules*, *39*, 7708–7717.

Karukatis, K. K., D'Angelo, N. D., & Loftus, C. T. (1997). Using the optical probe methyl orange to determine the role of surfactant and alcohol chain length in the association of 1-alkanols with alkyltrimethylammonium bromide micelles. *Journal of Physical Chemistry B*, *101*, 1968–1973.

Lesage, A., Steuerna, S., & Emsley, L. (1998). Carbon-13 spectral editing in solid-state NMR using heteronuclear scalar couplings. *Journal of American Chemistry Society*, *120*, 7095–7100.

Lin, Y., Liu, X., Dong, Z., Li, B., Chen, X., & Li, Y. S. (2008). Amphiphilic core-shell nanocarriers based on hyperbranched poly(ester amide)-star-PCL: Synthesis, characterization, and potential as efficient phase transfer agent. *Biomacromolecules*, *9*, 2629–2636.

Liu, X. M., Pramoda, K. P., Yang, Y. Y., Chow, S. Y., & He, C. (2004). Cholesteryl-grafted functional amphiphilic poly(*N*-isopropylacrylamide-*co*-*N*-hydroxylmethylacrylamide): Synthesis, temperature-sensitivity, self-assembly and encapsulation of a hydrophobic agent. *Biomaterials*, *25*, 2619–2628.

Ma, Y., Yi, J., & Zhang, L. (2009). A facile approach to incorporate silver nanoparticles into dextran-based hydrogels for antibacterial and catalytical application. *Journal of Macromolecular Science Part A*, *46*, 643–648.

Ma, Z., Zhao, S., Cheng, K., Zhang, X., Xu, X., & Zhang, L. (2007). Molecular weight and chain conformation of amylopectin from rice starch. *Journal Applied Polymer Science*, *104*, 3124–3128.

Miranda, J. A., Cacita, N., & Okano, L. T. (2007). Evaluation of amylopectin clusters and their interaction with nonionic surfactants. *Colloids and Surfaces B: Biointerfaces*, *60*, 19–27.

Prakash, I., Muralidharan, P., Nallamuth, N., Venkateswarlu, M., & Satyanarayana, N. (2007). Preparation and characterization of nanocrystallite size. *Materials Research Bulletin*, *42*, 1619–1624.

Rolland-Sabate, A., Colonna, P., Mendez-Montealvo, M. G., & Planchot, V. (2007). Branching features of amylopectins and glycogen determined by asymmetrical flow field flow fractionation coupled with multiangle laser light scattering. *Biomacromolecules*, *8*, 2520–2532.

Saha, A., & Ramakrishnan, S. (2009). Unimolecular micelles and reverse micelles based on hyperbranched polyethers – comparative study of AB_2 + A-R and $A_2 + B_3$ + A-R type strategies. *Journal of Polymer Science Part A: Polymer Chemistry*, *47*, 80–91.

Satoh, T. (2009). Unimolecular micelles based on hyperbranched polycarbohydrate cores. *Soft Matter*, *5*, 1972–1982.

Seth, D., Chakrabort, A., Setua, P., & Sarkar, N. (2006). Interaction of ionic liquid with water in ternary microemulsions (triton X-100/water/1-butyl-3-methylimidazolium hexafluorophosphate) probed by solvent and rotational relaxation of coumarin 153 and coumarin 151. *Langmuir*, *22*, 7768–7775.

Seiler, M., Rolker, J., & Arlt, W. (2003). Phase behavior and thermodynamic phenomena of hyperbranched polymer solutions. *Macromolecules*, *36*, 2085–2092.

Shen, Z., Chen, Y., Frey, H., & Stiriba, S. E. (2006). Complex of hyperbranched polyethylenimine with cuprous halide as recoverable homogeneous catalyst for the atom transfer radical polymerization of methyl methacrylate. *Macromolecules*, *39*, 2092–2099.

Slagt, M. Q., Stiriba, S. E., Gebbink, R. J. K., Kautz, H., Frey, H., & Koten, G. (2002). Encapsulation of hydrophilic pincer–platinum(II) complexes in amphiphilic hyperbranched polyglycerol nanocapsules. *Macromolecules*, *35*, 5734–5737.

Stiriba, S. E., Kautz, H., & Frey, H. (2002). Hyperbranched molecular nanocapsules: Comparison of the hyperbranched architecture with the perfect linear analogue. *Journal of American Chemistry Society*, *124*, 9698–9699.

Voit, B. I., & Lederer, A. (2009). Hyperbranched and highly branched polymer architectures synthetic strategies and major characterization aspects. *Chemical Reviewer*, *109*, 5924–5973.

Vriezema, D. M., Aragones, M. C., Elemans, J. A. A. W., Cornelissen, J. J. L. M., Rowan, A. E., & Nolte, R. J. M. (2005). Self-assembled nanoreactors. *Chemical Review*, *105*, 1445–1489.

Wan, D., Fu, Q., & Huang, J. (2006). Synthesis of amphiphilic hyperbranched polyglycerol polymers and their application as template for size control of gold nanoparticles. *Journal of Applied Polymer Science*, *101*, 509–514.

Wang, T. C., Rubner, M. F., & Cohen, R. E. (2002). Polyelectrolyte multilayer nanoreactors for preparing silver nanoparticle composites: Controlling metal concentration and nanoparticle size. *Langmuir*, *18*, 3370–3375.

Wilms, D., Wurm, F., Nieberle, J., Bohm, P., Kemmer-Jonas, U., & Frey, H. (2009). Hyperbranched polyglycerols with elevated molecular weights: A facile two-step synthesis protocol based on polyglycerol. *Macromolecules*, *42*, 3230–3236.

Wiltshire, J. T., & Qiao, G. G. (2007). Recent advances in star polymer design: Degradability and the potential for dug delivery. *Australia Journal of Chemistry*, *60*, 699–705.

Wu, D., Liu, Y., Jiang, X., Chen, L., He, C., Goh, S. H., et al. (2005). Evaluation of hyperbranched poly(amino ester)s of amine constitutions similar to polyethylenimine for DNA delivery. *Biomacromolecules*, *6*, 3166–3173.

Wu, J. (1994). *Technique and applications of modern FTIR spectroscopy*. Beijing: Science Press.

Yang, C., Meng, B., Chen, M., Liu, X., Hua, Y., & Ni, Z. (2006). Laser-light-scattering study of structure and dynamics of waxy corn amylopectin in dilute aqueous solution. *Carbohydrate Polymers*, *64*, 190–196.

Zhang, L., Yin, Q., Su, J., & Wu, Q. (2011). Local polarity and microviscosity of the interior of dendritic polyethylene amphiphiles. *Macromolecules*, *44*, 6885–6890.

Zhong, F., Yokoyama, W., Wang, Q., & Shoemaker, C. F. (2006). Rice starch, amylopectin and amylose: Molecular weight and solubility in dimethyl sulfoxide-based solvents. *J. Agric. Food Chem.*, *54*, 2320–2326.

Zou, J., Zhao, Y., & Shi, W. (2006). Encapsulation mechanism of molecular nanocarriers based on molecular micelle forming dendritic core-shell structural polymers. *Journal of Physical Chemistry B*, *110*, 2638–2642.